metals

MDPI

Article

Effects of High-Intensity Ultrasound on Microstructure and Mechanical Property of In situ TiB_2/2A14 Composites

Kai Huang [1,2], Ripeng Jiang [1,2,*], Xiaoqian Li [1,2,3], Lihua Zhang [2,3], Zhenghua Li [2,3] and Ruiqing Li [1,2,3]

1 Research Institute of Light Alloy, Central South University, Changsha 410083, China; csuhk1209@csu.edu.cn (K.H.); meel@csu.edu.cn (X.L.); lll87430@126.com (R.L.)
2 State Key Laboratory of High Performance Complex Manufacturing, Changsha 410083, China; zhanglihua@csu.edu.cn (L.Z.); lizhenghua0904@163.com (Z.L.)
3 College of Mechanical and Electrical Engineering, Central South University, Changsha 410083, China
* Correspondence: jiangrp@csu.edu.cn; Tel.: +86-151-7314-9455

Received: 19 October 2019; Accepted: 8 November 2019; Published: 11 November 2019

Abstract: In situ TiB_2/2A14 composites with a 3% volume fraction were prepared by mixing salt reaction and high energy ultrasound. The effects of high-intensity ultrasonic on the microstructure and mechanical properties of TiB_2/2A14 composites were systematically investigated. The microstructures of the composites were analyzed using scanning electron microscopy (SEM) and electron backscattered diffraction (EBSD). The phase composition was examined by X-ray diffraction (XRD) and energy dispersive spectroscopy (EDS). The results showed that after introducing ultrasonic vibration into the melt, due to the cavitation and acoustic streaming effect, the particle agglomerations were significantly reduced and particles of different sizes were evenly dispersed in the matrix. With ultrasonic vibration treatment of 120 s, the agglomerations were basically eliminated, and the particles were uniformly distributed to the most. The yield strength, tensile strength and elongation of the composites were increased by 53%, 21% and 30%, respectively, compared with that without ultrasonic vibration treatment (UVT).

Keywords: TiB_2 particles; aluminum matrix composite; ultrasonic; in situ reaction

1. Introduction

TiB_2 particle-reinforced aluminum matrix composites (AMC) have been widely used in aerospace and automotive industries due to their high specific modulus, high hardness, thermodynamic stability and low cost. According to the different ways of producing reinforcement phases in metal matrix composites, they can be divided into ex situ and in situ [1–5]. The principle of In situ reaction is to add a reactant capable of chemically reacting with the alloy matrix to form a desired reinforcement particle, thereby obtaining a particle-reinforced aluminum-based composite material. Compared with the ex situ, the particle size of the reinforced phase produced by the in situ is smaller, up to micron or even nanoscale. The micron particle has good compatibility and interfacial bonding with the matrix, and no pollution on the surface, which can further improve the properties of the composites [5–11].

At present, in situ synthesis methods of metal matrix composites mainly include self-propagating high temperature synthesis (SHS), exothermic dispersion (XD), contact reaction (CR), vapor-liquid reaction synthesis (VLS), mixed salt reaction (LSM), reactive spray deposition (RSD), etc.

Among them, the LSM method [12] is a patent technology invented by the London & Scandinavian Metallurgical (LSM) Company in England. The basic principle is that after pre-heat treatment at a specific temperature, the mixed salts containing Ti and B (such as KBF_4 and K_2TiF_6) are added to the

metal melt at high temperature. In situ TiB_2 reinforced metal matrix composites are obtained after solidification [12,13].

However, the particle reinforcement aluminum composites tend to agglomerate by traditional mechanical stirring. As an innovative process, high-energy ultrasonic treatment of metal melts has attracted wide attention due to its low cost, environmental friendliness and wide application in the treatment of aluminum alloy or other light alloy melts. Eskin et al. [14] studied the effect of ultrasound on SiC_P/Al-Si. It was found that the particle size of the composites treated by ultrasound was smaller, and the spatial distribution was more uniform. This phenomenon was attributed to the improvement in the wettability of the reinforcement particle and matrix by the ultrasonic cavitation, promoting the probability that the particles be captured and swallowed by the matrix during solidification. Liu et al. [15] studied the effect of ultrasound on the preparation of TiB_2/Al composites by the mixed salt reaction method. The results showed that ultrasound could reduce the reaction temperature of TiB_2/Al composites by 100 °C. Nampoothiri et al. [16] prepared Al-4.4 Cu/TiB_2 nanocomposites by the in situ reaction method. After melt being re-melted, the composites' melt was treated by ultrasonic vibration. It was found that the size of TiB_2 particles in the composites with ultrasonic vibration treatment (UVT) decreased significantly. The yield strength of the composites was about twice as large as the matrix alloys. Yang et al. [17,18] prepared TiCp/2219 composites with different volume fractions by semi-solid mixing through mechanical stirring and the ultrasonic vibration method. It was found that the micro-jet, high temperature and high pressure produced by the collapse of cavitation bubbles could fragment the inclusion layer of particle aggregates and scatter the particles agglomerations. Qi et al. [4]. obtained 2.5 Vol% TiB_2/Al-4.5Cu composites by a mixed salt reaction. The melt of composites was treated by ultrasound. It was found that ultrasound can effectively eliminate particle agglomeration and improve the mechanical properties of the composites. However, in the previous research, the underlying relationship between the distribution of particles and the mechanical properties were not clearly interpreted. Thus, the effect mechanism of UVT on microstructure formation, particle distribution and the mechanical properties of in situ, reinforced AMC, and was systematically studied in the paper.

2. Materials and Methods

In this experiment, 2A14 aluminum alloy was chosen as the matrix material. The chemical composition of 2A14 alloy was determined by optical emission spectroscopy (SPECTROMAXx, SPECTRO, Germany), as was shown in Table 1. The reactants involved in the formation of in situ TiB_2 particles are K_2TiF_6, KBF_4 and Na_3AlF_6 powders (purity: 99.5%), and were supplied by Shanghai Macklin reagent company.

Table 1. Chemical composition of 2A14 aluminum alloy (mass fraction,%).

Si	Cu	Mg	Zn	Mn	Ti	Ni	Fe	Al
0.90	4.55	0.63	0.019	0.76	0.031	0.015	0.099	Bal.

As shown in Figure 1, the main devices include the resistance furnace, graphite crucible, graphite agitator, drying furnace, graphite mold (specification Ø50 × 80 mm), Type-K thermocouple, temperature acquisition module, the laptop and ultrasonic system, etc. The ultrasonic casting apparatus is comprised of an in-house ultrasonic generator with a maximum output power of 2 kW, an air-cooled piezoelectric transducer (~20 kHz), an ultrasonic amplitude transformer and a cylindrical sonotrode (with a diameter of 25 mm).

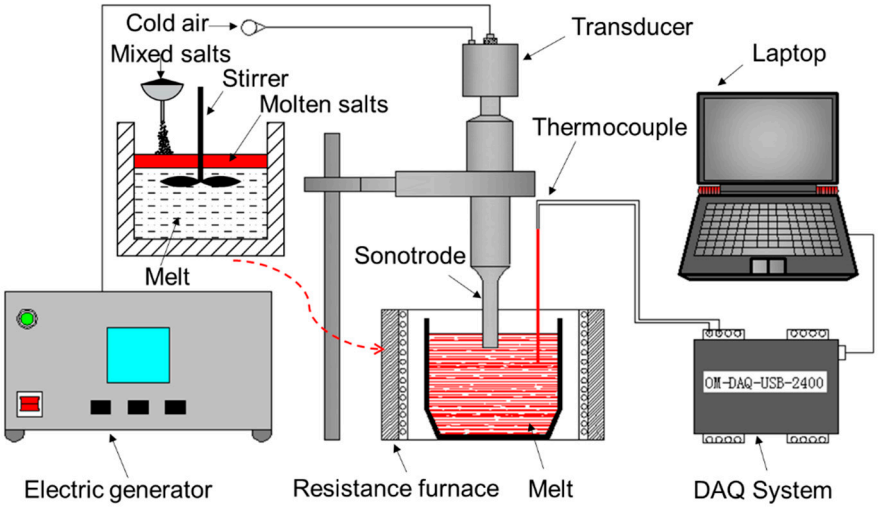

Figure 1. Schematic diagram of experiment.

The alloy 2A14 weighed about 500 g, was melted in a graphite crucible and heated in a resistance furnace to 820 °C. In order to prepare 3 vol % TiB_2 particulate reinforced composites, the mass of K_2TiF_6 and KBF_4 was weighed according to the atomic ratio of 1:2. The mass of the co-solvent Na_3AlF_6 is 10% of the total mass of the two reaction salts.

The TiB_2/2A14 composites were firstly fabricated by the salt reaction and mechanical stirring process. The resistance, graphite crucible and stirrer were applied, which were shown in Figure 1. The uniform and preheated salts powder was evenly added into the aluminum melt at 820 °C. Before the reaction completed, the melt temperature was controlled at 820 °C for 30 min with stirring. The prefabricated composites ingot was obtained by pouring aluminum melt into the graphite mold when the melt was cooled to 720 °C. The chemical reaction equation occurring in the melt is as follows [19,20]:

$$3K_2TiF_6 + 13Al \rightarrow 3KAlF_4 + K_3AlF_6 + 3Al_3Ti \quad (1)$$

$$2KBF_4 + 3Al \rightarrow 2KAlF_4 + AlB_2 \quad (2)$$

$$AlB_2 + Al_2Ti \rightarrow 4Al + TiB_2 \quad (3)$$

The above reactions can also be described as:

$$3K_2TiF_6 + 6KBF_4 + 10Al \rightarrow 3TiB_2 + 9KAlF_4 + K_3AlF_6 \quad (4)$$

The prefabricated composites material was re-melted by the graphite crucible and resistance furnace for the ultrasonic vibration treatment process. The ultrasonic vibration treatment experiment schematic is shown in Figure 1. The preheated ultrasonic sonotrode was immersed in 20 mm below the melt surface when the temperature of melt was stable at 720 °C. Meanwhile, the ultrasonic devices with power and frequency, 2 kW and 20 kHz, respectively, were switched on. The UVT time was set to 0 s, 30 s, 60 s, 120 s and 240 s, respectively. The temperature of this melt was recorded in real time and saved to the computer. The acquisition frequency was one second. After the UVT, the composites melt was poured into the preheated mold and cooled to obtain the final composite ingot.

The specimens of composites and matrix for metallographic and mechanical examination were prepared from the middle region of the ingot. The metallographic specimens were ground and polished following the standard metallographic procedure and etched by Keller's reagent. Grain size was measured using a linear intercept method (ASTM 112-10). The Al_2Cu phase and TiB_2 agglomerations were observed by field scanning emission electron microscopy (SEM; FESEM, MIRA3 TESCAN, Czech Republic) at 20 kV accelerating voltage and 15 mm working distance.

The Electron Backscatter Diffraction (EBSD) samples were ground and electro-polish in the solution of 30% nitric acid (HNO_3) and 70% methanol (CH_3OH) at 18 V for 50 s. EBSD was used to investigate the grain size and TiB_2 particle distribution. X-ray diffraction patterns were employed (XRD; D8 Advance, Bruker, Germany) with Cu Kα radiation in scan range of 2θ from 20° to 90° with an increment of 0.02°and a scanning speed of 2.4°/min. The power of an X-ray source was 600 W (30 Kv and 20 mA). XRD and energy dispersive spectroscopy (EDS; OXFORD 6650, IPG Photonics, Oxford, MS, USA) were used to identify the composition of phases. The ambient temperature (25 °C) tensile tests were carried out by a mechanical testing machine (America Instron 3369, Instron, Norwood, MA, USA) with a loading rate of 1 mm/min following the ASTM B557 Standard, and the fracture surface was observed by SEM (FESEM, MIRA3 TESCAN, Czech Republic). All the tests were performed thrice, and the mean value of the three results was used as the final result. The standard deviations were also calculated and showed in detail.

3. Results and Discussions

Figure 2a shows the XRD pattern of in situ TiB_2/2A14 composites. The diffraction peaks in the spectra are mainly TiB_2, Al_2Cu and Al. The in situ Al-Ti-B reaction system, the common Al_3Ti, AlB_2 and other intermediate alloys were not found in the spectrum. Due to the fact that the Gibbs free energy of TiB_2 is much lower than that of AlB_2 and Al_3Ti at the same temperature, the TiB_2 phase is more stable [15]. It is also proven that the Al- K_2TiF_6-KBF_4 has been thoroughly reacted. Figure 2b is the XRD spectrum with a diffraction angle from 39–39.5°. The lines in the graph are relatively smooth, and there are no obvious diffraction peaks. It proves that there is no Al_3Ti, which also verifies the research results of Gao et al. [4]. In addition to TiB_2, Al_2Cu and Al, alumina (Al_2O_3) also exists in the XRD spectrum. This may be due to the destruction of the oxide film on the surface of the aluminum melt by mechanical stirring, which results in the contact reaction between the aluminum melt and the air. The oxide film formed is involved in the melt and becomes the oxide inclusion phase of the composites.

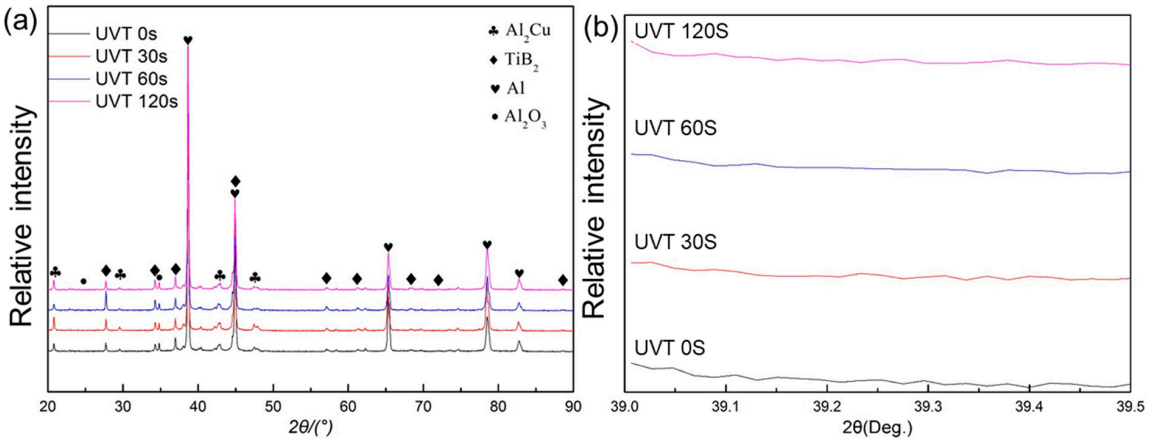

Figure 2. X-ray diffraction (XRD) pattern of TiB_2/2A14 composites: (**a**) diffraction angle from 20° to 90°; (**b**) diffraction angle from 39.0°to 39.5°.

Figure 3 shows the SEM results of the microstructures of the composites with different UVT durations, which reveals that UVT has obvious effects on the particles' distribution of in situ TiB_2 composites. As shown in Figure 3a, the smooth, thick and net-shape Al_2Cu phase exists in the alloy matrix. The micrograph of composites without UVT, as shown in Figure 3b, possessing a large agglomeration with size over 200 μm, can be found. These agglomerations are formed in the in situ reaction, and existed before solidification, which makes them barely affected by the solidification front. The large TiB_2 particle aggregates of composite with UVT for 30 s are dispersed into small particle aggregates with a size of about 50 μm, as shown in Figure 3c. The agglomeration of particles in the composites is further improved when the UVT time is extended to 60 s, as shown in Figure 3d. With

the UVT time increasing to 120 s, the large agglomerations were nearly eliminated, and some small agglomerations with the size under 20 μm can be observed as shown in Figure 3e. However, with prolonged UVT, particles agglomerate again when the UVT time reaches 240 s, as shown in Figure 3f. In this experiment, UVT of 120 s is the proper processing time.

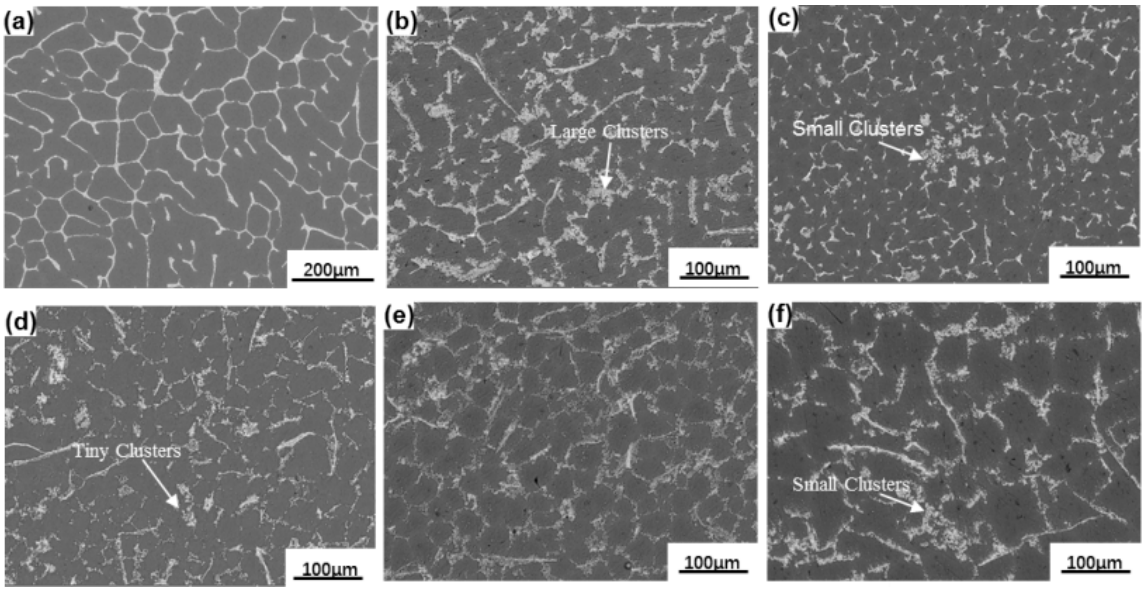

Figure 3. Microstructure of 2A14 matrix (**a**) and TiB_2/2A14 composites: (**b**) Without ultrasonic vibration treatment (UVT), (**c**) UVT for 30 s, (**d**) UVT for 60 s, (**e**) UVT for 120 s, (**f**) UVT for 240 s.

The distribution of TiB_2 particles near the grain boundary was observed by SEM in order to study the detailed effect of UVT. It can be seen that the fine TiB_2 particles gather near the white island Al_2Cu phase whose morphology is changed by the TiB_2 particles, as shown in Figure 4. There is a serious agglomeration near the grain boundary of the composites without UVT, and the size of island-like aggregates is about 40 μm as shown in Figure 4a. The agglomeration of particles near grain boundaries was obviously improved after a UVT of 30 s, as shown in Figure 4b. There are some irregular TiB_2 particles near the grain boundary when the UVT time increases to 60 s, as shown in Figure 4c. The TiB_2 agglomerations nearly disappear and many individual net-polygon particles scatter into the Al matrix with UVT of 60 s, which can obviously be observed in Figure 4d. The morphology of these TiB_2 particles is crucial for the mechanical properties of the composites [18]. Equiaxed and quasi-equiaxed symmetry shape of nano- or micro-particles are favorable as reinforced phases in in situ casting composites [5]. Figure 4d exhibits a well-developed hexagonal morphology of TiB_2 particles which are well embedded in the matrix, which will inhibit the crack propagation during ductile deformation, thus improving mechanical properties. This indicates that ultrasound not only can disperse the agglomeration of particles, but change the morphology of TiB_2 particles, which is beneficial for the improvement in the mechanical properties of the composite.

EBSD mapping was used to detect the matrix and composites to clearly characterize the grain size of the matrix. As shown in shown in Figure 5, the black spots are TiB_2 particles, which can be seen along the grain boundary, which is consistent with the results observed by SEM. Compared with Figure 5a,b, it can be observed that the grain size of the matrix alloy is obviously refined due to the presence of TiB_2 particles, which decreases from 224 μm to 46 μm, as shown in Figure 5f. This is due to the fact that the in situ TiB_2 particles can become heterogeneous nucleation sites of α-Al, which accelerates the nucleation rate of α-Al and inhibits the growth grains [21,22]. In Figure 5b, the area of black spots is larger, which indicates that the agglomeration of particles near the grain boundaries is serious without UVT. With the increase of the UVT time, the area of black spots decreases gradually, and the distribution of black spots becomes uniform. At the same time, the matrix grains are further

refined. When the UVT time reaches 120 s, the large area of black spots disappears basically, as shown in Figure 5e. Some fine black spots inset into the color patches and the size of the color patches reaches the minimum. This shows that the ultrasound has effectively scattered the agglomeration of TiB_2 particles. The particles enter into the matrix and the grain size is reduced to 28 μm.

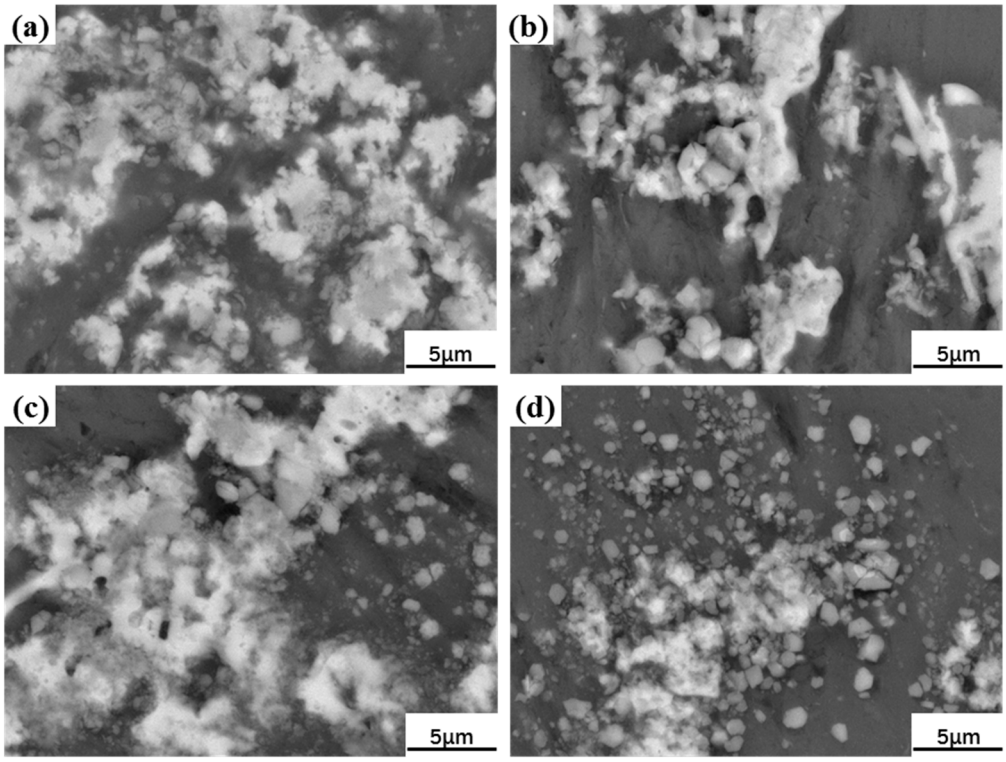

Figure 4. Microstructures of sub-micrometer particle agglomerations in composites with different UVT time: (**a**) 0 s, (**b**) 30 s, (**c**) 60 s and (**d**) 120 s.

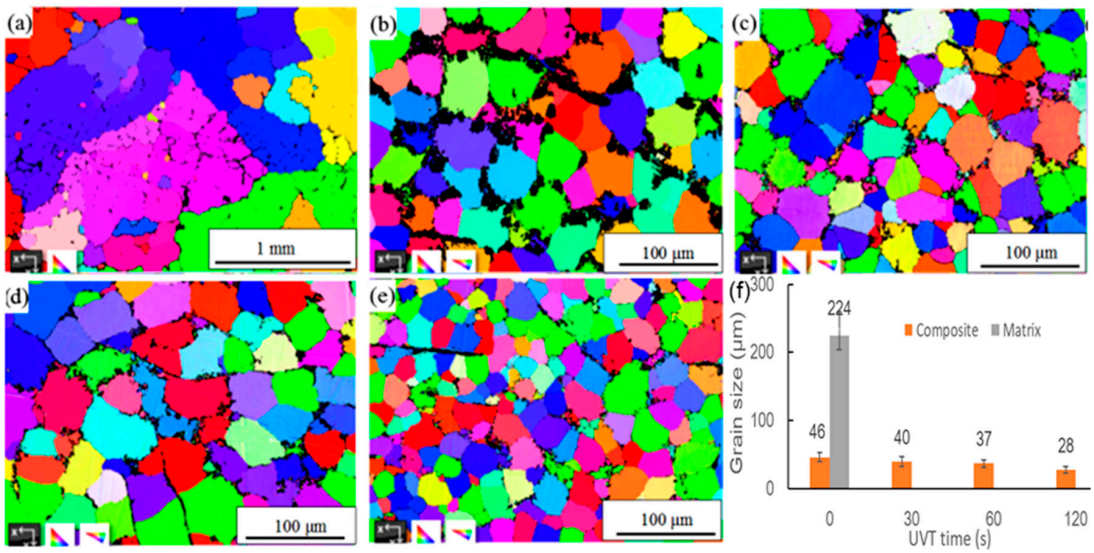

Figure 5. Electron backscattered diffraction (EBSD) (IPF X) images of TiB_2/2A14 composites with UVT. (**a**) 2A14 matrix alloy, (**b**) UVT for 0 s, (**c**) UVT for 30 s, (**d**) UVT for 60 s and (**e**) UVT for 120 s; (**f**) is the average grain size of the TiB_2/2A14 composites.

Figure 6 gives a schematic diagram of the ultrasonic effect in the TiB_2/2A14 composites' melt. The cavitation effect and the acoustic streaming effect play a key role in dispersing the agglomeration of particles in the composites' melt and promoting the uniform distribution of particles. Cavitation effect refers to the cavitation bubbles generated under the positive and negative sound pressure of ultrasound in the melt of composites. Cavitation bubbles grow spontaneously under the half-cycle negative pressure of ultrasound. When they collapse under the half-cycle positive pressure of ultrasound, they produce a high-intensity pressure pulse and high-speed micro-jet, which can directly act on the agglomerated particles and eliminate the phenomenon of particle aggregation. The intensity of the cavitation induced by ultrasonic vibration in the melt can be evaluated by the intensity of ultrasound. Its calculation formula is as follows [23]:

$$I = \frac{1}{2}\rho c(2\pi f A)^2 \tag{5}$$

where ρ is the density of melt, c is the propagation speed of ultrasound in the melt, f is the vibration frequency of ultrasound and A is the amplitude of ultrasound. The values of ρ, c, f and A are 2.7 g·cm^{-2}, 4.78×10^3 m/s, 20 kHz and 12 μm, respectively. By calculation, the intensity of ultrasound is about 1467 W/cm^2.

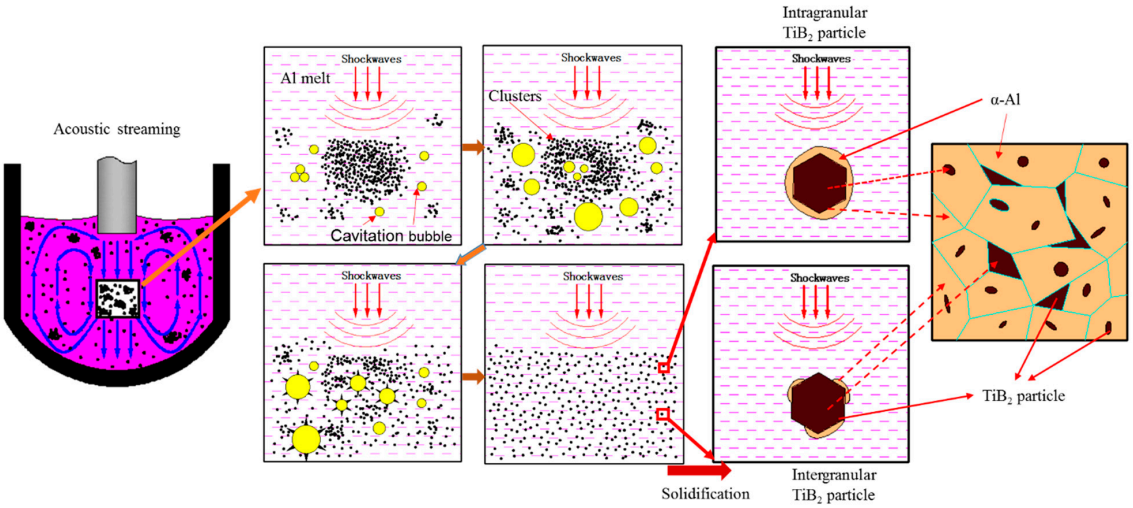

Figure 6. Schematic diagram of ultrasonic cavitation and acoustic streaming phenomenon in the TiB_2/2A14 composites melt.

Considering that the vibration energy of the ultrasonic sonotrode cannot be absorbed by the melt completely, and the loss of the vibration transmission process, the actual amplitude acting on the melt should be less than the calculated value. However, compared with the ultrasonic cavitation threshold ($I \geq 80$ W/cm^2) in the full cavitation state of the aluminum melt, the calculated ultrasonic intensity in formula (5) is much larger than the cavitation threshold [23,24]. Therefore, the ultrasonic cavitation effect can be greatly produced in the composites melt. Due to the viscous resistance of the composites melt, the sound pressure gradient is obvious when ultrasound propagates in the melt from the sound source, which causes the acoustic flow phenomenon [25]. TiB_2-agglomerated particles in composites melt are dragged to the area where ultrasonic cavitation is significant for dispersion and refinement. At the same time, the treated particles are diffused into the 2A14 alloy matrix again by the vortex caused by acoustic flow. Therefore, under the combined effect of cavitation and acoustic flow, the agglomeration of particles in the composite melt can be effectively scattered, and the fine particles can be dispersed into the alloy matrix. The dispersion effect of ultrasound on particle agglomeration is related to the intensity and action time of ultrasound. From formula (5), it can be inferred that increasing the frequency and amplitude of ultrasound vibration can improve the intensity of ultrasound, followed by

the processing time of ultrasound. According to the observation and analysis of the microstructure of TiB_2/2A14 composites, the dispersion effect of ultrasound on particles is not positively correlated with the UVT time. In this experiment, the optimal UVT time is 120 s. At the same time, UVT can also increase the wettability of TiB_2 particles and α-Al. During the solidification of composites, it is found that most TiB_2 particles can be captured and wrapped in the alloy matrix by the solidification front, while very few TiB_2 particles are pushed to the grain boundary by the solidification front, resulting in the agglomeration of TiB_2 particles, as shown in Figure 6.

Figure 7 shows the test results of the mechanical property of the 2A14 Alloy matrix and TiB_2/2A14 composites at room temperature. It can be seen that the yield strength and tensile strength of the composites have been greatly improved, which are 43% and 77% higher than that of 2A14 matrix, respectively. The yield strength and tensile strength of the composites increased with the prolongation of the UVT time, and the properties of the composites tend to be more stable. The mechanical property of the composites changes little when the UVT time is 30 s compared with composites without UVT. However, the yield strength and tensile strength of the composites reach 189 MPa and 325 MPa with the increase of the UVT time to 120 s. Compared with the composites without UVT, it is increased by 66 MPa and 56 MPa respectively, and the elongation increased from 7.9% to 10.3%, which is close to the elongation of the matrix.

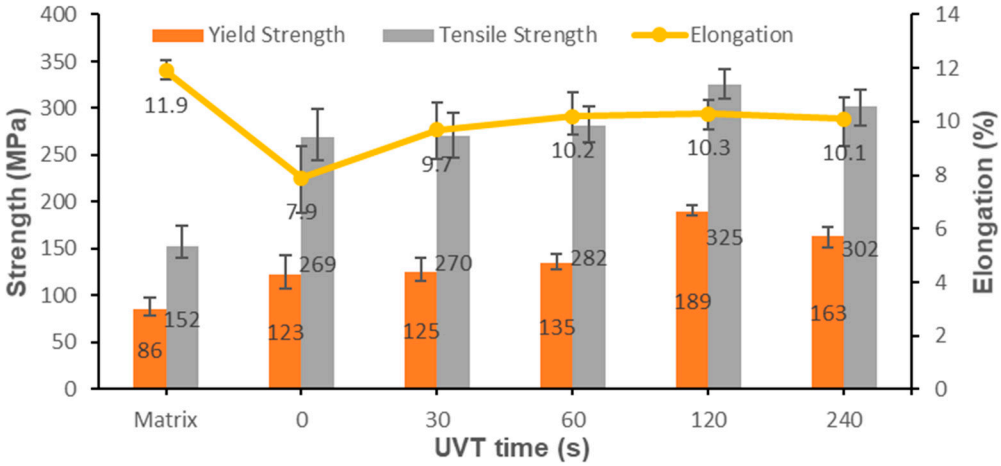

Figure 7. Mechanical properties of 2A14/TiB2 composites and matrix.

However, the mechanical properties of the composites are reduced when the UVT time increases to 240 s, which is consistent with the changing trend of the microstructure.

Figure 8 presents the tensile fracture morphology of the 2A14 alloy matrix and 3 vol % TiB_2/2A14 composite. In Figure 8a, a large area of flat cleavage surfaces presents on the fracture surface of 2A14 alloy matrix, dimples and tear edges appear in some areas, and cracks also exist. The fracture mechanism can be regarded as a brittle-plastic fracture. Figure 8b is the fracture morphology of the composites without UVT. The number of dimples on the fracture surface decreases obviously, and the shape area decreases. Because of the existence of particles, the large area of flat cleavage surface decreases. However, there are still a number of cleavage surfaces and tear edges in the partial region. The agglomeration of particles near the tear edge or in the large dimple is serious. In the local region, due to crack expansion, void areas are formed. As a result, the elongation decreases significantly from 11.9% to 7.9% of the matrix, and the fracture mechanism is a brittle-plastic mixed fracture [26]. Figure 8c is the fracture morphology of composites with UVT for 30 s. There are large voids at the fracture surface. This is because when ultrasound is applied, the melt level will be disturbed, gas or oxide inclusions will be introduced, which reduces the interfacial bonding ability between particles and the matrix. When the composites are subjected to external loading, some agglomerated particles will fall off from the matrix, resulting in a large volume of voids at the fracture surface, so the elongation of

the composite decreases significantly, from 11.9% of the matrix to 9.7%. The fracture mechanism is brittle-plastic mixed fracture. Figure 8d is the fracture morphology of the composite with UVT for 60 s. Both tear edges and cleavage faces exist, which belong to quasi cleavage fracture [27]. After UVT for 60 s, the particle agglomeration at the fracture is reduced, and the cracks near the tearing edge are decreased. However, the particle agglomeration still exists in dimples, so the elongation is decreased to 10.2%. Figure 8e shows the fracture morphology of composites with UVT of 120 s. It can be seen that the agglomeration of particles in the composites is basically eliminated and the cracks are reduced. The brittle flat cleavage surface is also reduced, while the number of tearing edges and dimples is increased. The dimples are smaller and shallower and distributed evenly on the fracture surface, showing obvious dimple fracture characteristics. As a result, the elongation decreases slightly, from 11.9% of the matrix to 10.3%. Figure 8f is a high magnification image of area A in Figure 8e, in which a large number of small dimples and particles are observed around the tearing edge.

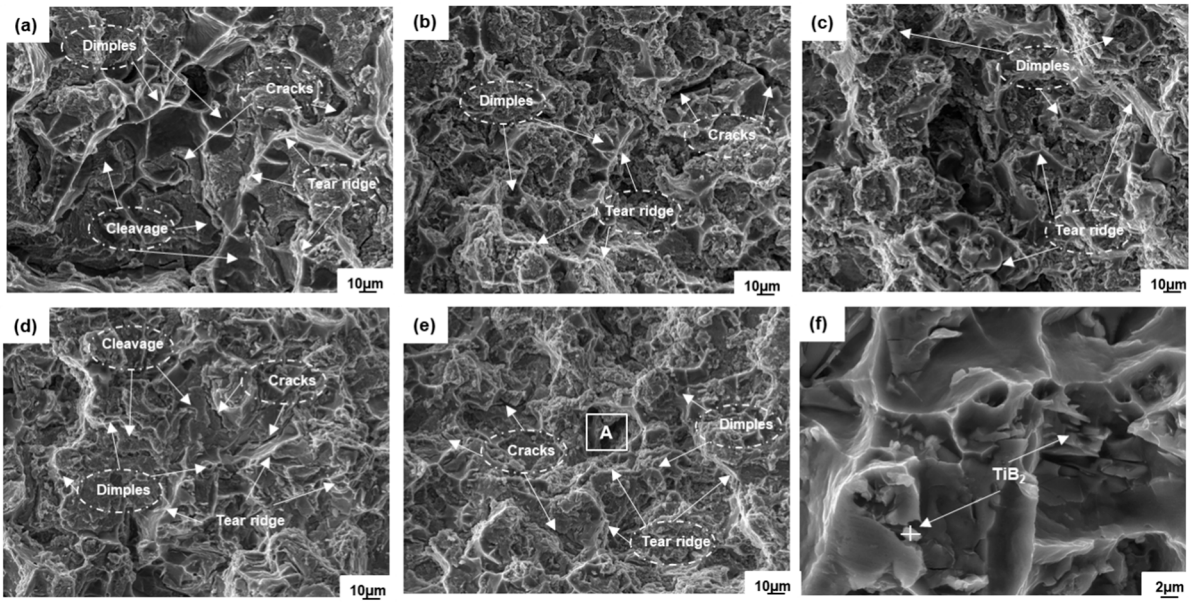

Figure 8. Tensile samples fracture surface morphology of (**a**) 2A14 alloy matrix, (**b**) TiB_2/2A14 composites without UVT, (**c**) TiB_2/2A14 composites with UVT for 30 s, (**d**) TiB_2/2A14 composites with UVT for 60 s, (**e**) TiB_2/2A14 composites with UVT for 120 s and (**f**) high magnification of A area.

EDS analysis of the particles of composite with UVT for 120 s shows that there are a large number of sub-micron TiB_2 particles in the dimple, which are in good shape and did not crack in the dimple, as shown in Figure 9. Some very small dimples are also found, and TiB_2 particles are not found at the bottom of the dimples. The dimple size is similar with particles outside the dimples. This shows that TiB_2 particles are pulled out of the matrix under the action of external loading in the region where the interface binding capacity is weak, which is a typical case when the particles separate from the matrix interface. Besides, the presence of these particles will affect the morphology and size of the dimples and cleavage surfaces, and ultimately affect the tensile strength of the composites [28]. Fractured particles exist in dimples or near tearing edges, which indicates that after UVT for 120 s, the particles are bonded tightly with the matrix. When subjected to external loading, the particles rupture due to loading, thus improving the mechanical properties of the composites.

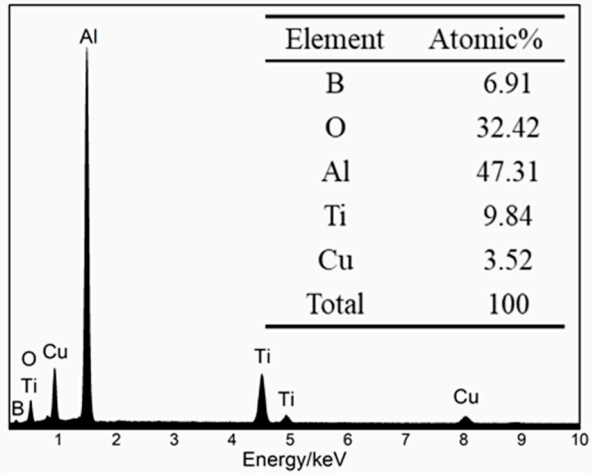

Figure 9. Energy dispersive spectroscopy (EDS) analysis of the TiB_2 particle (white point in Figure 8f) of TiB_2/2A14 composites.

The increase of elongation of composites with UVT is attributed to the improvement of ductility of composites [29–31] by grain refinement and the uniform dispersion of TiB_2 in composites. First, the grain refinements can produce more grains in composites. During tensile deformation, these grains can disperse stress, produce more uniform plastic deformation and reduce the stress concentration [31]. Secondly, grain refinement can produce more curved grain boundaries, which can hinder crack growth. Thirdly, TiB_2 particles in composites can change the direction of crack growth and produce bridging, branching and deflection of cracks. During the process of crack transfer and deflection, a large amount of energy will be absorbed, which will hinder the growth of cracks and increase the elongation of composites [31]. Therefore, the elongation of TiB_2 composites can be significantly improved by the fine and uniformly-distributed TiB_2 particles under the action of ultrasound.

4. Conclusions

TiB_2/2A14 composites were successfully prepared by a mixed salt reaction assisted by UVT. UVT can effectively improve the distribution of particles. Large-volume agglomerated particles are scattered into small-volume aggregated or dispersed particles by high-pressure shock wave, and evenly spread to the melt through acoustic streaming. SEM and EBSD results indicate that when the UVT time is 120 s, the agglomeration of TiB_2 is basically eliminated, and the particles are evenly distributed near the boundary of the refined grains or into the grain interior.

The mechanical properties of as-cast TiB_2/2A14 composites were improved. The yield strength, tensile strength and elongation of the composites with UVT for 120 s are 53%, 21% and 30%, respectively, being higher than those of the composites without UVT. With the increase of ultrasonic treatment time, the agglomeration of particles on the fracture surface of composites decreases due to the good bonding ability between particles and matrix.

Author Contributions: Conceptualization, R.J. and X.L.; Methodology, K.H. and R.J.; software, K.H.; Validation, R.L., L.Z. and Z.L.; Formal analysis, R.J. and K.H.; Investigation, K.H.; Resources, R.J. and X.L.; Data curation, R.J.; Writing—original draft preparation, K.H.; Writing—review and editing, R.J.; Visualization, K.H.; Supervision, R.J.; Project administration, R.J.; Funding acquisition, R.J. and L.Z.

Funding: This research was funded by the National Natural Science Foundation of China, Grant number: 51805549 and 51575539, Hunan Natural Science Foundation, Grant number: 2017JJ3391.

Conflicts of Interest: The authors declare no conflict of interest.

References

1. Clyne, T.W.; Withers, P.J. *An Introduction to Metal. Matrix Composites*; Cambridge University Press: Cambridge, UK, 1993.
2. Tjong, S.C.; Ma, Z.Y. Microstructural and mechanical characteristics of in situ metal matrix composites. *Mater. Sci. Eng. R Rep.* **2000**, *29*, 49–113. [CrossRef]
3. Ibrahim, I.A.; Mohamed, F.A.; Lavernia, E.J. Particulate reinforced metal matrix composites—A review. *J. Mater. Sci.* **1991**, *26*, 1137–1156. [CrossRef]
4. Gao, Q.; Wu, S.; Lv, S.; Xiong, X.; Du, R.; An, P. Improvement of particles distribution of in situ 5 vol% TiB_2 particulates reinforced Al-4.5Cu alloy matrix composites with ultrasonic vibration treatment. *J. Alloys Compd.* **2017**, *692*, 1–9. [CrossRef]
5. Wang, T.; Chen, Z.; Zheng, Y.; Zhao, Y.; Kang, H.; Gao, L. Development of TiB_2 reinforced aluminum foundry alloy based in situ composites-Part II: Enhancing the practical aluminum foundry alloys using the improved Al–5 wt% TiB_2 master composite upon dilution. *Mater. Sci. Eng. A* **2014**, *605*, 22–32. [CrossRef]
6. Karbalaei Akbari, M.; Baharvandi, H.R.; Shirvanimoghaddam, K. Tensile and fracture behavior of nano/micro TiB_2 particle reinforced casting A356 aluminum alloy composites. *Mater. Des.* **2015**, *66*, 150–161. [CrossRef]
7. Kandemir, S.; Atkinson, H.V.; Weston, D.P.; Hainsworth, S.V. Thixoforming of A356/SiC and A356/TiB_2 Nanocomposites Fabricated by a Combination of Green Compact Nanoparticle Incorporation and Ultrasonic Treatment of the Melted Compact. *Metall. Mater. Trans. A* **2014**, *45*, 5782–5798. [CrossRef]
8. Kumar, S.; Chakraborty, M.; Sarma, V.S.; Murty, B.S. Tensile and wear behaviour of in situ Al–7Si/TiB_2 particulate composites. *Wear* **2008**, *265*, 134–142. [CrossRef]
9. Iqbal, N.; Van Dijk, N.H.; Offerman, S.E.; Moret, M.P.; Katgerman, L.; Kearley, G.J. Real-time observation of grain nucleation and growth during solidification of aluminium alloys. *Acta Mater.* **2005**, *53*, 2875–2880. [CrossRef]
10. Gao, Q.; Wu, S.; Lv, S.; Duan, X.; An, P. Preparation of in situ 5 vol% TiB_2 particulate reinforced Al–4.5 Cu alloy matrix composites assisted by improved mechanical stirring process. *Mater. Des.* **2016**, *94*, 79–86. [CrossRef]
11. Xue, J.; Wang, J.; Han, Y.; Li, P.; Sun, B. Effects of CeO_2 additive on the microstructure and mechanical properties of in situ TiB_2/Al composite. *J. Alloys Comp.* **2011**, *509*, 1573–1578. [CrossRef]
12. Daries, P.; Kellief, J.L.F.; Wood, J.V. Metal matrix alloys. UK Patent 2257985A, 1992.
13. Wang, H.-W.; Li, X.-F.; Ma, N.-H.; Wang, P. Method of Preparing Aluminum Matrix Composites Via Salts-Metal Reaction. China Patent CN03115677.0, 27 August 2003.
14. Eskin, G.I.; Eskin, D.G. Production of natural and synthesized aluminum-based composite materials with the aid of ultrasonic (cavitation) treatment of the melt. *Ultrason. Sonochem.* **2003**, *10*, 297–301. [CrossRef]
15. Liu, Z.; Rakita, M.; Xu, W.; Wang, X.; Han, Q. Ultrasound assisted salts–metal reaction for synthesizing TiB_2 particles at low temperature. *Chem. Eng. J.* **2015**, *263*, 317–324. [CrossRef]
16. Nampoothiri, J.; Harini, R.S.; Nayak, S.K.; Raj, B.; Ravi, K.R. Post in situ reaction ultrasonic treatment for generation of Al–4.4 Cu/TiB_2 nanocomposite: A route to enhance the strength of metal matrix nanocomposites. *J. Alloys Comp.* **2016**, *683*, 370–378. [CrossRef]
17. Yang, Y.; Liu, Z.; Jiang, R.; Li, R.; Li, X. Microstructural evolution and mechanical properties of the AA2219/TiC nanocomposite manufactured by ultrasonic solidification. *J. Alloys Comp.* **2019**, *811*, 1–12. [CrossRef]
18. Yang, Y.; Jiang, R.; Li, X.; Zhang, Y.; Li, R. Effect of Nanoparticle Content on the Microstructural and Mechanical Properties of Forged and Heat-Treated TiC/2219 Nanocomposites. *Metals* **2019**, *982*, 1–14. [CrossRef]
19. Emamy, M.; Mahta, M.; Rasizadeh, J. Formation of TiB_2 particles during dissolution of $TiAl_3$ in Al–TiB_2 metal matrix composite using an in situ technique. *Compos. Sci. Technol.* **2006**, *66*, 1063–1066. [CrossRef]
20. Chen, F.; Chen, Z.; Mao, F.; Wang, T.; Cao, Z. TiB_2 reinforced aluminum based in situ composites fabricated by stir casting. *Mater. Sci. Eng. A* **2015**, *625*, 357–368. [CrossRef]
21. Xie, M.Y.; Ao, S.H.; Wang, X. Effect of Al5Ti1B master alloy on microstructure and mechanical properties of Al-5 wt.% Cu based alloy. *Adv. Mater. Res.* **2014**, *1051*, 195–198. [CrossRef]
22. Wang, C.; Wang, M.; Yu, B.; Chen, D.; Qin, P.; Feng, M.; Dai, Q. The grain refinement behavior of TiB_2 particles prepared with in situ technology. *Mater. Sci. Eng. A* **2007**, *459*, 238–243. [CrossRef]

23. Liu, Z.; Han, Q.; Li, J. Ultrasound assisted in situ technique for the synthesis of particulate reinforced aluminum matrix composites. *Compos. Part. B Eng.* **2011**, *42*, 2080–2084. [CrossRef]
24. Yang, Y.; Lan, J.; Li, X. Study on bulk aluminum matrix nano-composite fabricated by ultrasonic dispersion of nano-sized SiC particles in molten aluminum alloy. *Mater. Sci. Eng. A* **2004**, *380*, 378–383. [CrossRef]
25. Eskin, G.I.; Eskin, D.G. *Ultrasonic Treatment of Light Alloy. Melts*, 1st ed.; CRC Press: Boca Raton, FL, USA, 1998.
26. Zhang, Z.; Topping, T.; Li, Y.; Vogt, R.; Zhou, Y.; Haines, C.; Paras, J.; Kapoor, D.; Schoenung, J.M.; Lavernia, E.J. Mechanical behavior of ultrafine-grained Al composites reinforced with B4C nanoparticles. *Scr. Mater.* **2011**, *65*, 652–655. [CrossRef]
27. Han, G.; Zhang, W.; Zhang, G.; Feng, Z.; Wang, Y. High-temperature mechanical properties and fracture mechanisms of Al-Si piston alloy reinforced with in situ TiB_2 particles. *Mater. Sci. Eng. A* **2015**, *633*, 161. [CrossRef]
28. Hu, Z.; Li, X.; Yan, H.; Wu, X.; Qun, H.; Lin, J. Effects of ultrasonic vibration on microstructure evolution and elevated-temperature mechanical properties of hot-extruded Mg-6Al-0.8Zn-2.0Sm wrought magnesium alloys. *J. Alloys Comp.* **2016**, *685*, 58–64. [CrossRef]
29. Fang, C.; Wang, L.; Hao, H.; Zhang, X. Distribution of TiB_2 reinforcements in magnesium matrix composites by a multi-physical coupling field. *J. Mater. Process. Technol.* **2014**, *214*, 551–555. [CrossRef]
30. Fang, C.; Liu, G.; Hao, H.; Zhang, X. Effects of particle distribution on microstructural evolution and mechanical properties of TiB_2/AZ31 composite sheets. *Mater. Sci. Eng. A* **2017**, *684*, 592–597. [CrossRef]
31. Tian, K.; Zhao, Y.; Jiao, L.; Zhang, S.; Zhang, Z.; Wu, X. Effects of in situ generated ZrB_2 nano-particles on microstructure and tensile properties of 2024Al matrix composites. *J. Alloys Comp.* **2014**, *594*, 1–6. [CrossRef]